

# Dynamic of Stochastic Gradient Descent with State-Dependent Noise

Qi Meng<sup>1</sup>\*, Shiqi Gong<sup>2</sup>, Wei Chen<sup>1</sup>, Zhi-Ming Ma<sup>2</sup>, Tie-Yan Liu<sup>1</sup>

<sup>1</sup>Microsoft Research Asia, <sup>2</sup>University of Chinese Academy of Sciences

## Abstract

Stochastic gradient descent (SGD) and its variants are mainstream methods to train deep neural networks. Since neural networks are non-convex, more and more works study the dynamic behavior of SGD and the impact to its generalization, especially the escaping efficiency from local minima. However, these works take the over-simplified assumption that the covariance of the noise in SGD is (or can be upper bounded by) constant, although it is actually state-dependent. In this work, we conduct a formal study on the dynamic behavior of SGD with state-dependent noise. Specifically, we show that the covariance of the noise of SGD in the local region of the local minima is a quadratic function of the state. Thus, we propose a novel power-law dynamic with state-dependent diffusion to approximate the dynamic of SGD. We prove that, power-law dynamic can escape from sharp minima exponentially faster than flat minima, while the previous dynamics can only escape sharp minima polynomially faster than flat minima. Our experiments well verified our theoretical results. Inspired by our theory, we propose to add additional state-dependent noise into (large-batch) SGD to further improve its generalization ability. Experiments verify that our method is effective.

## 1 Introduction

Deep learning has achieved great success in various AI applications, such as computer vision, natural language processing, and speech recognition [11, 28, 7]. Stochastic gradient descent (SGD) and its variants are the mainstream methods to train deep neural networks, since they can deal with the computational bottleneck of the training over large-scale datasets [1].

Although SGD can converge to the minimum in convex optimization [20], neural networks are highly non-convex. On one hand, researchers are investigating the loss surface of the neural networks with variant architectures [3, 14, 9, 4]; on the other hand, it is empirically shown that, the noise in SGD serves as an implicit regularization and will make SGD stop at local minima with different generalization ability [13, 8, 36]. Moreover, the empirical results show that SGD with relatively larger noise (by decreasing batch size) will stop at flatter minima. Obviously, whether SGD can escape poor local minima and finally stop at the minimum with low loss and good generalization ability is crucial to its test performance. Thus, more and more works study dynamic behavior of SGD in non-convex optimization and its impact on generalization.

These works consider SGD as the discretization of a continuous-time dynamic system and investigate its dynamic properties, especially the escaping efficiency from local minima. For example, [15, 34, 17, 2, 8, 36, 12, 32] approximate the dynamic of SGD by Langevin dynamic with constant diffusion coefficient and proved its the escaping efficiency from local minima. In the work [29, 6], state-dependent noise of SGD has been studied, but there's no analysis on the escaping efficiency for it. [24, 23] assume the variance of stochastic gradient is infinite and use  $\alpha$ -stable process to

\*Corresponding E-mail: meq@microsoft.com

approximate the dynamic of SGD. They proved a faster escaping efficiency in the sense that the escaping time from a basin is independent with the barrier height. However, these works take the over-simplified assumption that, the noise in SGD is independent with the parameters of the model.

In this work, we conduct a formal study on the (state-dependent) noise structure of SGD and its dynamic behavior. First, we show that the covariance of the noise of SGD in the quadratic basin surrounding the local minima is a quadratic function of the state, i.e., the parameters of the model. Thus, we propose approximating the dynamic of SGD near the local minimum using a stochastic differential equation with state-dependent diffusion. We call the new dynamic *power-law dynamic*, since we prove that the distribution of the state is power-law distribution.

Second, we analyze the dynamic properties of power-law dynamic, especially the escaping efficiency from local minima. By using the random perturbation theory for diffused dynamic systems, we analyze two kinds of escaping efficiency of the power-law dynamic: the  $\epsilon$ -escaping time of a dynamic to escape the  $\epsilon$ -wide region of a minimum; and the  $\Omega$ -escaping time to escape from one basin with surrounding surface  $\Omega$  to another. We prove that, in terms of two escaping time, the escaping time of power-law dynamic is exponentially decreasing as the noise-to-signal ratio of the second-order derivatives tends to large. As smaller noise-to-signal ratio of the derivatives leads to better generalization [16], we can conclude that power-law dynamic can escape from worse-generalized minima exponentially faster than better-generalized minima. Moreover, the  $\Omega$ -escaping time for power-law dynamic is only in the polynomial order of the barrier height, much faster than the exponential order in previous work. Thus our results can better explain that SGD implicitly tends to learn well-generalized minima.

Finally, we corroborate our theory by experiments. We first calculate the covariance of noise in SGD on neural networks, and observe that it can be well approximated by quadratic function of the parameters. We then compare the escaping efficiency of dynamics with constant diffusion coefficient or state-dependent diffusion coefficient to that of SGD. We observed that, the dynamic with state-dependent covariance diffusion can escape local minima faster and is more consistent with the escaping behavior of SGD. Inspired by our theory, we propose to add additional state-dependent noise into (large-batch) SGD to further improve its generalization ability. Experiments on image classification tasks verify that our method can achieve lower generalization error and higher test accuracy compared to SGD.

## 2 Background

We focus on the adoption of optimization algorithms to solve the following empirical risk minimization problem, whose objective is

$$L(w) := \frac{1}{n} \sum_{m=1}^n \ell(x_m, w), \quad (1)$$

where  $\{x_m | m = 1, \dots, n\}$  denotes the training dataset with  $n$  *i.i.d.* training samples,  $w \in \mathbb{R}^d$  denotes the parameters of the model and  $\ell$  denotes the loss function.

A typical approach to minimize Eq.(1) is gradient descent (GD) whose update rule is  $w_{t+1} = w_t - \eta \nabla_w L(w_t)$ , where  $\eta$  denotes the learning rate. In practice, a more useful kind of gradient based optimizers is stochastic gradient descent (SGD),

$$w_{t+1} = w_t - \eta g(w_t), \quad (2)$$

where  $g(w_t) = \frac{1}{b} \sum_{x \in S_b} \nabla_w \ell(x, w_t)$  is an unbiased estimator of the full gradient  $\nabla_w L(w_t)$ , with  $S_b$  being a randomly sampled minibatch of size  $b$ . According to Central Limit Theorem, the stochastic gradient  $g(w_t)$  asymptotically follows Gaussian distribution [15], i.e.,  $g(w_t) - \nabla L(w_t) \sim \mathcal{N}(0, \Sigma(w_t))$ .  $\Sigma(w_t) = \frac{1}{b} \left( \frac{1}{n} \sum_{m=1}^n \nabla \ell(x_m, w_t) \nabla \ell(x_m, w_t)^T - \nabla L(w_t) \nabla L(w_t)^T \right)$  is the covariance matrix of the stochastic gradient  $g(w_t)$ . For small enough constant learning rate  $\eta$ , Eq.(2) can be treated as the numerical discretization of the following stochastic differential equation (SDE) [15],

$$dw_t = -\nabla_w L(w_t) dt + \sqrt{\eta \Sigma(w_t)}^{1/2} dB_t, \quad (3)$$

where  $B_t$  is a standard Brownian motion in  $\mathbb{R}^d$ . Under the assumption that  $\nabla_w L(w_t)$  and  $\Sigma(w_t)^{1/2}$  are Lipschitz continuous function about the state  $w_t$ , the SDE is a Itô drift-diffusion process. The

vector  $\nabla_w L(w_t)$  is known as the drift coefficient of  $w$ ; the matrix  $\sqrt{\eta}\Sigma(w_t)^{1/2}$  is known as the diffusion coefficient of  $w$ .

As stated in the introduction, the covariance  $\Sigma(w_t)$  is assumed to be constant or upper bounded by some constant (i.e.,  $\Sigma(w_t) = \Sigma$  or  $\Sigma(w_t) < \Sigma$ ) in many literatures. When  $\Sigma(w_t)$  is constant, the dynamic of Eq.(3) is known as the Langevin dynamic [21]. Different from previous works, we are the first to study the dynamic of SGD with state-dependent noise.

**Notations:**  $Cov(\cdot, \cdot)$  and  $Var(\cdot)$  denotes the covariance of two random variables and the variance of a random variable respectively, and all the expectations are taken over the empirical distribution on training samples. We use  $diag(a_1, \dots, a_d)$  to denote a diagonal matrix with diagonal elements  $a_1, \dots, a_d$ , and use the subscript  $i$  (or  $j$ ) to denote the  $i$  (or  $j$ )-th element of a vector or a diagonal matrix. Except for the stochastic gradient, the letter with upper wave line  $\tilde{\cdot}$  denotes the stochastic version of a function which is calculated by a mini-batch of data.  $B(a, b)$  and  $\Gamma(a)$  denotes the Beta function and Gamma function respectively, and they satisfies  $B(a, b) = \frac{\Gamma(a)\Gamma(b)}{\Gamma(a+b)}$ .

### 3 Approximating SGD by Power-law Dynamic

In this section, we study the (state-dependent) noise structure of SGD in the quadratic basin and propose power-law dynamic to approximate the dynamic of SGD.

#### 3.1 Noise Structure of Stochastic Gradient Descent

We first describe the loss curvature of the quadratic basin we aim to study. We assume  $w^*$  is a local minimum of the loss function that satisfies the first-order stationary condition:  $\nabla_w L(w^*) = 0$ , and the loss function in the region  $[w^* - \epsilon, w^* + \epsilon]$  with  $\epsilon > 0$  can be approximated by second-order Taylor expansion as  $L(w) \approx L(w^*) + \frac{1}{2}(w - w^*)^T H(w - w^*)$ . Here,  $H$  is the Hessian matrix of loss at  $w^*$ . We call  $\epsilon$  as width of the basin and  $\max_{w \in [w^* - \epsilon, w^* + \epsilon]} L(w) - L(w^*)$  as height of the basin. Without loss of generality, we assume  $L(w^*) = 0$  and  $H = diag(h_1, \dots, h_d)$  in the following context. The diagonal Hessian assumption is widely adopted for theoretical analyses, e.g., in [22, 33, 30]. The gradient of  $L(w)$  is  $\nabla L(w) = H(w - w^*)$ , and  $\nabla_j L(w) = h_j(w_j - w_j^*)$ .

We use  $\tilde{L}(w)$  to denote a stochastic version of  $L(w)$ , i.e., the loss composed by a minibatch of data. The second-order Taylor expansion of  $\tilde{L}(w)$  is

$$\tilde{L}(w) = g(w^*)(w - w^*) + \frac{1}{2}(w - w^*)^T \tilde{H}(w - w^*), \quad (4)$$

where  $g(w^*)$  and  $\tilde{H}$  are unbiased estimator of  $\nabla L(w^*)$  and  $H$ . The gradient of  $\tilde{L}(w)$  is  $g(w) = g(w^*) + \tilde{H}(w - w^*)$ . The randomness of  $g(w)$  comes from two parts:  $g(w^*)$  and  $\tilde{H}$ , which corresponds to the fluctuation of the first-order and second-order derivative of the model at  $w^*$  on different training samples, respectively. So because of the term  $\tilde{H}(w - w^*)$ , the covariance matrix of  $g(w)$  is independent with  $w$  if and only if  $\tilde{H} = H$ . That means, the Hessian matrix at  $w^*$  for all training samples are equal, which is not true in general. Actually, every element in the covariance matrix is a quadratic function of  $w_1, \dots, w_d$ . For analytic tractability, we study a simplified version of state-dependent covariance matrix as shown in Proposition 1.

**Proposition 1** *We use  $D(w)$  to denote the covariance matrix of stochastic gradient  $g(w) = g(w^*) + \tilde{H}(w - w^*)$  and  $\tilde{H} = diag(\tilde{h}_1, \dots, \tilde{h}_d)$  is diagonal. If  $Cov(\tilde{h}_i, \tilde{h}_j) = 0$  for  $i \neq j$ ,  $Cov(g_i(w^*), g_j(w^*)) = 0$  for  $i \neq j$  and  $Cov(g_i(w^*), \tilde{h}_j) = 0, \forall i, j$ , we have  $D(w) = diag(D_1, \dots, D_d)$  with*

$$D_j = \sigma_j + \rho_j(w_j - w_j^*)^2, \quad (5)$$

where  $\sigma_j = Var(g_j(w^*))$  and  $\rho_j = Var(\tilde{h}_j)$ .

We use linear regression to illustrate that when the conditions in Proposition 1 can be easily satisfied.

**Example:** Consider linear regression with loss function  $L(w) = \frac{1}{2n} \sum_{m=1}^n (x_m w - y_m)^2 = \frac{1}{2n} \|Xw - Y\|_2^2$ . We suppose the output  $y$  is generated as:  $y = w'x + \epsilon$  where  $\epsilon$  is a standard

Gaussian random variable, which is independent with the distribution of the input  $x$ . The stochastic gradient at the empirical minimizer  $w^*$  is calculated as  $g(w^*) = \frac{1}{b} \tilde{H}(w^* - w') - \frac{1}{b} \tilde{X}^T \tilde{\epsilon}$ . We can prove that the conditions on  $Cov(\tilde{h}_i, \tilde{h}_j)$ ,  $Cov(g_i(w^*), g_j(w^*))$  and  $Cov(g_i(w^*), \tilde{h}_j)$  in Proposition 1 can be satisfied if  $Cov(X_i, X_j) = \frac{1}{n} \sum_{m=1}^n x_{m,i} x_{m,j} - (\frac{1}{n} \sum_{m=1}^n x_{m,i})(\frac{1}{n} \sum_{m=1}^n x_{m,j}) = 0, i \neq j$  and the training data is sufficiently large such that  $w^* - w' \approx 0$ . We put the proof in the Appendix.

### 3.2 Power-Law Dynamic

In this section, we study the dynamic of SGD with covariance  $D(w) = \text{diag}(D_1, \dots, D_d)$  as described in Eq.(5). Under the condition that the Hessian is diagonal, the loss function around  $w^*$  decomposes as a sum of scalar quadratic function for each coordinate:  $L(w) \approx \frac{1}{2} \sum_{j=1}^d h_j (w_j - w_j^*)^2$ . Then by using SGD, each dimension evolves independently as

$$w_{t+1,j} = w_{t,j} - (g_j(w^*) + \tilde{h}_j(w_{t,j} - w_j^*)). \quad (6)$$

We use two random variables  $\xi_1, \xi_2$  to model the noisy term  $\tilde{h}_j - h_j$  and  $g_j(w^*)$ . By central limit theorem,  $\xi_1$  and  $\xi_2$  are asymptotically distributed from Gaussian distribution  $\xi_1 \sim N(0, \rho_j)$  and  $\xi_2 \sim N(0, \sigma_j)$ , if we assume that they have finite variance. The update rule of SGD in Eq.(6) can be regarded as discretization of the following continuous-time dynamic,

$$dw_t = -H(w_t - w^*)dt + \sqrt{\eta D(w_t)} dB_t \quad (\text{power-law dynamic}) \quad (7)$$

We name the dynamic described in Eq.(7) "power-law dynamic" because the distribution density of  $w_t$  for solving Eq.(7) follows the power-law distribution as shown in the next proposition.

**Proposition 2** Suppose  $w_t$  satisfies the power-law dynamic in Eq.(7), and the initial point is  $w_0$ . The distribution density of  $w_t$  is  $p(w, t) = \prod_{j=1}^d p(w_j, t)$ , where

$$p(w_j, t) = Z_j(t)^{-1} [1 + \beta_j(t) \kappa_j (w_j - \hat{w}_j(t))^2]^{-\frac{1}{\kappa_j}} \quad (8)$$

with  $\kappa_j = \frac{\eta \rho_j}{h_j}$ ,  $\hat{w}_j(t) = w_j^* + (w_{0,j} - w_j^*) e^{-h_j t}$ ,  $Z_j(t) = [-\frac{1}{K_j} e^{-t/c_j} + \frac{1}{K_j}]^{\frac{1}{2-\kappa_j}}$ ,  $K_j = \frac{h_j}{2\eta \sigma_j \gamma_j}$ ,  $c_j = \frac{1}{h_j(2-\kappa_j)}$ ,  $\beta_j(t) = \gamma_j \left( \frac{1}{Z_j(t)} \right)^2$ ,  $\gamma_j = \frac{(B(\frac{1}{2}, \frac{1}{\kappa_j} - \frac{1}{2}))^2}{\kappa_j}$ .

We put the proof of Proposition 2 to the Appendix, which is based on the work [26]. The density function in Eq.(8) is called power-law  $\kappa_j$ -distribution [35] and  $Z_j(t)$  is the normalizing term of the density. The stationary-state solution of Eq.(7) is  $p(w_j) = Z_j^{-1} (1 + \beta_j \kappa_j (w_j - w_j^*)^2)^{-\frac{1}{\kappa_j}}$  with  $\beta_j = \frac{h_j}{\eta \sigma_j}$  [5]. As  $\kappa_j \rightarrow 0$ , the distribution density tends to be Gaussian, i.e.,  $p(w_j) \propto \exp(-\beta_j (w_j - w_j^*)^2)$ . In statistical physics, if we regard  $w_t$  as a particle in a thermal system follows Eq.(7),  $\kappa_j$  measures the distance away from the thermal equilibrium [35]. In the approximation of dynamic of SGD,  $\kappa_j$  equals to  $\frac{\eta \rho_j}{h_j}$ , which is the inverse of the signal-to-noise ratio (SNR) of the Hessian at  $w^*$ . Compared to Gaussian distribution, the decay of the probability density as  $w$  goes to infinity of power-law dynamic is slower. Thus power-law distribution produces higher probability to appear values far away from the center  $w^*$  compared to Gaussian distribution. Next, we will analyze the escaping efficiency from local minima for power-law dynamic.

## 4 Escaping Efficiency of Power-law Dynamic

In this section, we analyze the behavior of escaping from minima of power-law dynamic. Specifically, we analyze the  $\epsilon$ -escaping time and the  $\Omega$ -escaping time of power-law dynamic in Section 4.1 and Section 4.2 respectively.

### 4.1 $\epsilon$ -escaping time

First, we adopt the assumption describe in previous section that  $w^*$  is a local minimum of the loss function  $L(w)$  and  $L(w) \approx \frac{1}{2} (w - w^*)^T H(w - w^*)$ . We introduce the definition of  $\epsilon$ -escaping time.

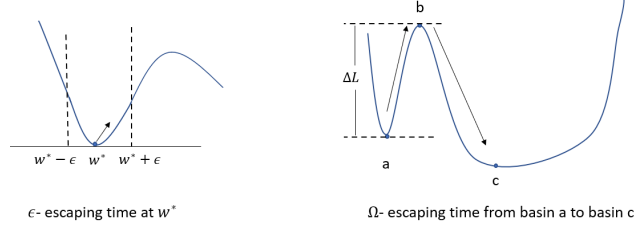


Figure 1: The left figure illustrates the setting of the  $\epsilon$ -escaping time which only depends on curvature in a small region around local minimum  $w^*$ . The right figure illustrates the setting of the  $\Omega$ -escaping time which depends on the curvature of the basin where  $a$  is located.

**Definition 3** Suppose we start a dynamic from the minimum  $w^*$ . For a fixed positive constant  $\epsilon > 0$ , we call the time  $t$  to make  $\mathbb{E}_{w_t}[\|w_t - w^*\|^2] = \epsilon^2$ , the  $\epsilon$ -escaping time.

**Remark:**  $\epsilon$ -escaping time is an equivalent variation of escaping efficiency defined in the work [36]. We measure the escaping efficiency according to the width of the local region, while they use height of the local region in [36].

$\epsilon$ -escaping time describes the time to escape a small region around  $w^*$  and there's no further assumption on the loss curvature outside this small region, which is illustrated in the left figure in Figure.1. The next theorem gives the  $\epsilon$ -escaping time for power-law dynamic.

**Theorem 4** Suppose that  $w_t$  follows the power-law dynamic defined in Eq.(7). We have  $\mathbb{E}[\|w_t - w^*\|^2] = \mathcal{O}(\sum_{j=1}^d (\eta\sigma_j t)^{\frac{2}{2-\kappa_j}})$ , where  $\kappa_j = \frac{\eta\rho_j}{h_j} < \frac{2}{3}$ . The upper bound for  $\epsilon$ -escaping time is  $\mathcal{O}\left(\frac{\epsilon^{2-\min_j \kappa_j}}{Tr(\Sigma)}\right)$ , where  $\Sigma = diag(\eta\sigma_1, \dots, \eta\sigma_d)$  and  $Tr(\cdot)$  denote the trace of the matrix.

The proof for Theorem 4 is based on the distribution of  $w_t$  described in Proposition 2. According to Proposition 2, we can obtain the second-order moment of  $w_t - w_j^*$ , that is,

$$\mathbb{E}[\|w_t - w_j^*\|^2] = \sum_{j=1}^d \int_{-\infty}^{\infty} (w_{t,j} - w_j^*)^2 \cdot Z_j(t)^{-1} [1 + \beta_j(t)\kappa_j(w_{t,j} - w_j^*)^2]^{-\frac{1}{\kappa_j}} dw_{t,j}. \quad (9)$$

We put the calculation of Eq.(9) to the Appendix. Based on Theorem 4, we compare the  $\epsilon$ -escaping time for power-law dynamic and Langevin dynamic.

**Comparison with result for Langevin dynamic:** The  $\epsilon$ -escaping time for Langevin dynamic (i.e., the dynamic with constant coefficient  $\Sigma$  of the diffusion term) is  $\mathcal{O}(\epsilon^2/Tr(\Sigma))$  [36]. Compared to the result for Langevin dynamic, we have the following conclusions: (1) As  $\kappa_j \rightarrow 0$  for all  $j$ , the  $\epsilon$ -escaping time for power-law dynamic tends to that for Langevin dynamic. (2) The  $\epsilon$ -escaping time for power-law dynamic depends exponentially on  $\kappa_j$ . Specifically, we consider the  $\epsilon$ -escaping time along one dimension, which is  $\frac{1}{\eta\sigma_j} \cdot \epsilon^{2-\kappa_j}$ . Since  $\kappa_j = \frac{\eta\rho_j}{h_j}$  and  $\kappa_j$  is the noise to signal ratio of the  $h_j$ . As shown in [16], smaller  $\kappa_j$  leads to better generalization. We can conclude that power-law dynamic escapes worse-generalized minima exponentially faster than well-generalized minima, while Langevin dynamic can not reflect this. So power-law dynamic can better explain the regularization effect of SGD.

## 4.2 $\Omega$ -Escaping Time

In this section, we analyze the mean escaping time for  $w_t$  to escape from a basin to its neighbor basin. As shown in Figure.1, we suppose that there are two basins whose bottom are denoted as  $a$  and  $c$  respectively and  $b$  is the boundary between two basins. We denote  $\Omega$  to be the surface surrounding basin  $a$  and we call the mean escaping time as  $\Omega$ -escaping time for distinguishing from setting in previous section.

**Definition 5** Suppose  $w_t$  starts at  $a$ , we denote the time for  $w_t$  to first reach  $b$  as  $\inf\{t > 0 | w_0 = a, w_t > b\}$ . The  $\Omega$ -escaping time  $\tau$  is defined as  $\tau = \mathbb{E}_{w_t}[\inf\{t > 0 | w_0 = a, w_t > b\}]$ .

Type of Dynamics	$\epsilon$ -escaping time	$\Omega$ -escaping time (1-dim) (with barrier height $\Delta L = L(b) - L(a)$ )
Langevin dynamic[36]	$\mathcal{O}(\epsilon^2 / Tr(\Sigma))$	$\times$
Langevin dynamic[32]	$\times$	$\mathcal{O}\left(\exp\left(\frac{\Delta L}{\Sigma}\right)\right)$
$\alpha$ -stable process[19]	$\times$	$\mathcal{O}(\alpha \cdot  b - a ^\alpha)$
Power-law dynamic (ours)	$\mathcal{O}\left(\frac{\epsilon^{2-\min_j \kappa_j}}{Tr(\Sigma)}\right)$	$\mathcal{O}(1 + (\eta\mu\Sigma^{-1} * \Delta L)^{\frac{1}{\eta\mu} - \frac{1}{2}})$

Table 1: Recent quantitative research on escaping time analysis of SGD.  $\Sigma$  denotes the state-independent part in the covariance of stochastic gradient,  $\alpha$  denotes the index in  $\alpha$ -stable process. As for  $\kappa_j$  and  $\mu$ , readers can refer to Theorem 4 and Eq.(10). In [24, 19], the result of  $\alpha$ -stable process is only for 1-dimensional case. So we only show 1-dimensional result in the table for all the three dynamics for fair comparison.

For loss surface around the local minimum  $a$ , we adopt the same setting with that for  $w^*$  in Section 3.1, that is: the loss of a point near  $a$  is  $L(w) \approx \frac{1}{2}(w - a)^T H_a (w - a)$ . For the saddle point  $b$ , we suppose  $\nabla L(b) = 0$  and there is only one negative eigenvalue for  $H_b$ , which is denoted as  $h_{be}$ . We use  $\Delta L = \sum_{j=1}^d \Delta \ell_j = \sum_{j=1}^d \ell_j(b_j) - \ell_j(a_j)$  to denote the barrier height, in which we also adopt the assumption that each coordinate evolves independently.

The power-law dynamic in Eq.(7) only describes the dynamic in region around  $a$ . To make it adapt to the whole escaping path, we reformulate the power-law dynamic as following:

$$dw_t = -\nabla L(w_t)dt + \sqrt{\eta D(w_t)}dB_t, \quad (10)$$

where  $D(w) = \text{diag}(D_1, \dots, D_d)$ , and  $D_j = \mu_j \ell_j(w_{t,j}) + \sigma_j$ . It is consistent with the power-law dynamic defined in Eq.(7) if  $\mu_j = \frac{2\rho_j}{h_{a,j}}$ .

In order to analytically solve the  $\Omega$ -escaping time, we take the common *low temperature* assumption [32, 35], i.e.,  $\eta\sigma_j \ll \Delta \ell_j$ . The assumption can be satisfied when the learning rate is small. Under the low temperature assumption, we first give the  $\Omega$ -escaping time for 1-dimensional case in the following theorem and then extend it to high-dimensional case.

**Theorem 6** *The  $\Omega$ -escaping time of the power-law dynamic in Eq.(10) is as below,*

$$\tau = \frac{2\pi}{(1 - \frac{\eta\mu}{4})\sqrt{H_a|H_b|}} \left(1 + \frac{\mu}{\sigma}\Delta L\right)^{\frac{2}{\eta\mu} - \frac{1}{2}}. \quad (11)$$

**Proof:** The probability density of Power-law dynamic satisfies the Smoluchowski equation as

$$\begin{aligned} \frac{\partial p(w, t)}{\partial t} &= \frac{\partial}{\partial w} (\nabla L(w) \cdot p(w, t)) + \frac{\partial}{\partial w} \left( \phi(w) \frac{\partial p(w, t)}{\partial w} \right) \\ &= \frac{\partial}{\partial w} \left( \phi(w) \cdot \left(1 + \frac{\mu}{\sigma}L(w)\right)^{-\frac{1}{\kappa}} \frac{\partial \left( \left(1 + \frac{\mu}{\sigma}L(w)\right)^{\frac{1}{\kappa}} p(w, t) \right)}{\partial w} \right), \end{aligned}$$

where  $\kappa = \frac{\eta\mu}{2}$  and  $\phi(w) = \frac{\eta D(w)}{2}$ . According to Eq.(12) in [35], the escaping time  $\tau$  satisfies the following equation:  $\left(1 + \frac{\mu}{\sigma}L(w)\right)^{\frac{1}{\kappa}} \frac{\partial}{\partial w} \left( D(w) \cdot \left(1 + \frac{\mu}{\sigma}L(w)\right)^{-\frac{1}{\kappa}} \right) \frac{\partial \tau(w)}{\partial w} = -1$ . Thus we have

$$\tau = \int_w^b \phi(w')^{-1} \left(1 + \frac{\mu}{\sigma}L(w')\right)^{\frac{1}{\kappa}} \left( \int_a^{w'} \left(1 + \frac{\mu}{\sigma}L(w'')\right)^{-\frac{1}{\kappa}} dw'' \right) dw'$$

Assuming the loss at the basin has a minimum  $L(a)$  and  $L(w) \approx L(a) + \frac{1}{2}H_a(w - a)^2$ , and the loss at the basin has a maximum  $L(b)$  and it is written as  $L(w) \approx L(b) - \frac{1}{2}|H_b|(w - b)^2$ . Using this

approximation, we have

$$\begin{aligned}
\int_w^b \phi(w')^{-1} \left(1 + \frac{\mu}{\sigma} L(w')\right)^{\frac{1}{\kappa}} dw' &= \frac{2}{\eta\sigma} \int_w^b \left(1 + \frac{\mu}{\sigma} L(w')\right)^{-1+\frac{1}{\kappa}} dw' \\
&= \frac{2}{\eta\sigma} \int_{-\infty}^b \left(1 + \frac{\mu}{\sigma} (L(b) - \frac{1}{2}|H_b|(w' - b)^2)\right)^{-1+\frac{1}{\kappa}} dw' \\
&= \frac{2}{\eta\sigma} \left(1 + \frac{\mu}{\sigma} L(b)\right)^{-1+\frac{1}{\kappa}} \int_c^b \left(1 - \frac{\mu}{\sigma} \cdot \frac{\frac{1}{2}|H_b|(w' - b)^2}{1 + \frac{\mu}{\sigma} L(b)}\right)^{-1+\frac{1}{\kappa}} dw' \\
&= \frac{4}{\eta\sigma} \left(1 + \frac{\mu}{\sigma} L(b)\right)^{-1+\frac{1}{\kappa}} \cdot \left(\frac{\frac{1}{2}\frac{\mu}{\sigma}|H_b|}{1 + \frac{\mu}{\sigma} L(b)}\right)^{-1/2} \int_0^1 y^{-1/2} (1 - y)^{-1+\frac{1}{\kappa}} dy \\
&= \frac{4}{\eta\sigma} \left(1 + \frac{\mu}{\sigma} L(b)\right)^{-\frac{1}{2}+\frac{1}{\kappa}} \sqrt{\frac{2}{\mu\sigma|H_b|}} B\left(\frac{1}{2}, \frac{1}{\kappa}\right),
\end{aligned}$$

where  $B(a, b) = \frac{\Gamma(a)\Gamma(b)}{\Gamma(a+b)}$  is the Beta function. For the term  $\int_a^{w'} \left(1 + \frac{\mu}{\sigma} L(w'')\right)^{-\frac{1}{\kappa}} dw''$ , we have

$$\int_a^{w'} \left(1 + \frac{\mu}{\sigma} L(w'')\right)^{-\frac{1}{\kappa}} dw'' = \left(1 + \frac{\mu}{\sigma} L(a)\right)^{\frac{1}{2}-\frac{1}{\kappa}} \sqrt{\frac{2\sigma}{\mu H_a}} B\left(\frac{1}{2}, \frac{1}{\kappa} - \frac{1}{2}\right).$$

Combining the above equations, we can get the result in the theorem.

**Comparison with results for other dynamics:** The  $\Omega$ -escaping time for Langevin dynamic with constant diffusion coefficient is studied in [32], which is  $\frac{2\pi}{\sqrt{H_a|H_b|}} \exp\left(\frac{\Delta L}{\eta\sigma}\right)$ . Compared to the Langevin dynamic, we have the following conclusions: (1) When  $\mu \rightarrow 0$ , the  $\Omega$ -escaping time for power-law dynamic tends to that for Langevin dynamic. (2) Compared to the result for Langevin dynamic, power-law dynamic improves the order of barrier height (i.e.,  $\Delta L$ ) in  $\Omega$ -escaping time from exponential to polynomial, which implies a faster escaping efficiency of SGD to escape deep basin. (3) Since  $\mu$  is proportional to  $\frac{\eta\rho}{H_a}$  (noise-to-signal ratio of  $H_a$ ) and smaller noise-to-signal ratio leader to better generalization performance [16], the power-law dynamic can escape worse-generalization minima exponentially faster than better-generalized minima.

As shown in Table 1, the  $\Omega$ -escaping time for 1-dimensional  $\alpha$ -stable process is  $\mathcal{O}(\alpha \cdot |b - a|^\alpha)$ , which is independent with the barrier height but in polynomial order of the width of the basin. However, using  $\alpha$ -stable process to approximate the dynamic of SGD is based on a strong assumption that the variance of stochastic gradient is infinite. Compared to  $\alpha$ -stable process, the result for power-law dynamic is superior in the sense that it is also in polynomial order of the width (if  $\Delta L = (|b - a|^c)$ ,  $c > 0$ ) and power-law dynamic does not need the infinite variance assumption.

**Extension to high-dimensional case:** To extend the  $\Omega$ -escaping time to high-dimensional case, according to [27],  $\Omega$ -escaping time  $\tau$  can be expressed as  $\tau = \frac{P(w \in V_a)}{\int_\Omega J d\Omega}$ , where  $V_a$  is the volume of basin  $a$ ,  $J$  is the probability current produced by  $P(w \in V_a)$  and  $\int_\Omega J d\Omega$  is the probability flux (surface integrals of probability current). So we need to calculate  $P(w \in V_a)$  and  $\int_\Omega J d\Omega$  respectively. Under the low temperature assumption, the probability current concentrates along the direction corresponding the negative eigenvalue of  $H_b$  (i.e.,  $h_{be}$ ), which is the escaping direction, and the probability flux of other directions can be ignored. We put the result and detailed proof for high-dimensional case in Theorem 10 in Appendix.

## 5 Experiments

In this section, we conduct experiments to verify the theoretical results. First, we evaluate whether the quadratic approximation of the stochastic gradient is accurate on neural network models. Second, we count escaping frequency for dynamics with different diffusion terms and SGD. Besides, we propose to add additional state-dependent noise into (large-batch) SGD and conduct experiments to verify its effectiveness on image classification task.

## 5.1 Covariance of the Stochastic Gradient

In this section, we evaluate the quadratic approximation of covariance of the stochastic gradient on plain convolutional neural network (CNN) and ResNet. The structure for plain CNN model is  $input \rightarrow Conv1 \rightarrow maxpool \rightarrow Conv2 \rightarrow maxpool \rightarrow fc1 \rightarrow Relu \rightarrow fc2 \rightarrow output$ . we randomly sample 1000 images from FashionMNIST [31] dataset as training set. As for ResNet, we use the ResNet-18 model [11] and randomly sample 1000 images from Kaggle’s dogs-vs-cats dataset as training set. For each model, we use gradient descent with small constant learning rate to train the network till it converges. The converged point can be regarded as a local minimum, denoted as  $w^*$ . We put the detailed training strategies in Appendix.

We then calculate the covariance matrix of the stochastic gradient at some points belonging to the local region around  $w^*$ . The points are selected according to the formula:  $w_{layerL}^* \pm (i \times Scale)$ , where  $w_{layerL}^*$  denotes the parameters at layer  $L$ , and  $i \times Scale, i \in [N]$  determines the distance away from  $w_{layerL}^*$ . When we select points according to this formula by changing the parameters at layer  $L$ , we fixed the parameters at other layers. For both CNN model and ResNet18 model, we select 20 points by setting  $i = 1, \dots, 10$ . For example, for CNN model, we choose the 20 points by changing the parameters at the *Conv1* layer with  $Scale = 0.001$  and *Conv2* layer with  $Scale = 0.0001$ , respectively. For ResNet18, we choose the 20 points by changing the parameters for a convolutional layer at the first residual block with  $Scale = 0.0001$  and second residual block with  $Scale = 0.0001$ , respectively.

The results are shown in Figure.2. The x-axis denotes the distance of the point away from the local minimum and the y-axis shows the value of the trace of covariance matrix at each point. The results show that the covariance of noise in SGD is indeed not constant and it can be well approximated by quadratic function of state (the blue line in the figures), which is consistent with our theoretical results in Section 3.1.

## 5.2 Escaping efficiency on 2-D Model

In this section, we use a 2-dimensional (2-D) model to simulate the escaping efficiency from minima for power-law dynamic, Langevin dynamic and SGD. We design a non-convex function written as  $\ell(w) = 15 \sum_{j=1}^2 |w_j - 1|^{2.5} \cdot |w_j + 1|^3$ . Our loss function is  $L(w) = \frac{1}{n} \sum_{m=1}^n \ell(w - x_m)$ , where training data  $x_i \sim \mathcal{N}(0, 0.01I_2)$  and  $n = 100$ . There are 4 basins in the loss surface with corresponding local minimum  $(1, 1), (1, -1), (-1, 1)$  and  $(-1, -1)$ , as shown in Figure 3(a). Here, we analyze the behaviors of escaping from the minimum  $w^* = (1, 1)$ . We also plot the trace of covariance matrix of stochastic gradient around  $w^*$  in Figure.3(b) and it can be well approximated by a quadratic function.

We regard the following optimization iterates as the discretization of the power-law dynamic,

$$w_{t+1} = w_t - \eta \nabla L(w_t) + \eta \lambda_1 |w_t - w^*| \odot \xi_1 + \eta \lambda_2 \xi_2 \quad \textbf{(power-law)} \quad (12)$$

where  $\xi_1, \xi_2 \sim \mathcal{N}(0, I)$ ,  $\lambda_1$  are constant and  $\odot$  stands for Hadamard product. Note that if we set  $\lambda_1 = 0$  in Eq.(12), we have the algorithm,  $w_{t+1} = w_t - \eta \nabla L(w_t) + \eta \lambda_2 \xi_2$ , which can be regarded as discretization of Langevin dynamic. We set learning rate  $\eta = 0.025$ , and we take 500 iterations in each training. In order to match the trace of covariance matrix of stochastic gradient at minimum point  $w^*$  with the methods above,  $\lambda_2$  is chosen to satisfy  $Tr(Cov(\lambda_2 \xi_2)) = Tr(Cov(g(w^*)))$ .

We compare the success rate of escaping for power-law dynamic, Langevin dynamic and SGD by repeating the experiments 100 times. To analyze the noise term  $\lambda_1$ , we choose different  $\lambda_1$  and evaluate corresponding success rate of escaping, as shown in Figure.3(c). The results show that there is a positive correlation between  $\lambda_1$  and the success rate of escaping, and our proposed method work can better mimic the escaping efficiency of SGD than Langevin dynamic.

We then scale the loss function by 0.9 and the loss surface becomes flatter. We run all the algorithms under the same setting with the experiments on the un-scaled loss  $L(w)$ . The success rate of escaping is reported at Figure.3(d). We can observe that all dynamics escape sharp minima faster.

## 5.3 Image Classification on Cifar10

As shown in many literatures[13, 8], SGD with large batch generalizes worse. Motivated by our theoretical characterization on noise in SGD, we propose PL-SGD algorithm by adding both state-



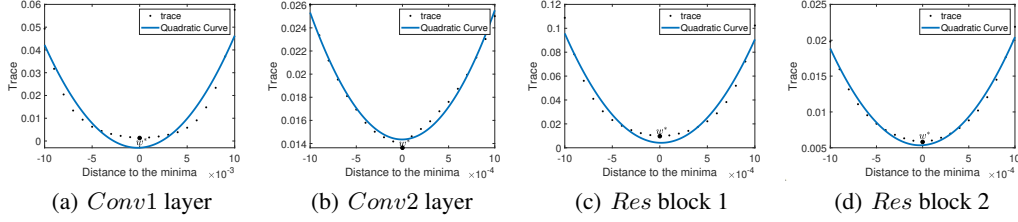


Figure 2: **(a),(b):** Trace of covariance matrix of stochastic gradient on CNN model. **(c),(d):** Trace of covariance matrix of stochastic gradient on ResNet18.

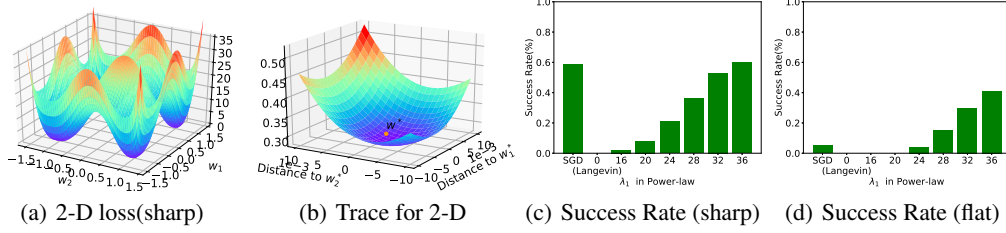


Figure 3: 2-D model. **(a):** Surface of the loss function  $L(w)$  for 2-D model. **(b):** Trace of covariance matrix around minimum  $(1, 1)$ . **(c):** Success rate of escaping from the basin of  $L(w)$  in repeated 100 runs. **(d):** Success rate of escaping from the basin of  $0.9L(w)$  in repeated 100 runs.

dependent and state-independent noise in SGD (shown in Eq.( )) to verify whether it can improve the test performance of SGD with large batch size.

$$w_{t+1} = w_t - \eta g(w_t) + \eta |w_t| \odot \xi_1 + \eta \xi_2. \quad (\text{PL-SGD}) \quad (13)$$

, where  $\xi_1 \sim \mathcal{N}(0, \lambda_1 I_d)$  and  $\xi_2 \sim \mathcal{N}(0, \lambda_2 I_d)$  and  $\lambda_1, \lambda_2$  are two hyper-parameters to tune. We compare PL-SGD to SGD and also compare it to SGLD [18] (as shown in Eq.) on CIFAR-10 with ResNet-18 model.

$$w_{t+1} = w_t - \eta g(w_t) + \eta \xi_3. \quad (\text{SGLD}) \quad (14)$$

where  $\xi_3 \sim \mathcal{N}(0, \lambda_3 I_d)$  and  $\lambda_3$  is a hyper-parameter to tune. The batch size for the three algorithms are set to be 2048. We train the three algorithms for 90 epochs. The initial learning rate is set to be 0.1 and is annealed to be 0.01 after 45 epochs. For PL-SGD, we tune  $\lambda_1$  and  $\lambda_2$  using grid search and report the best result in terms of test accuracy, which is achieved at  $\lambda_1 = 0.02$  and  $\lambda_2 = 1e - 4$ . For SGLD, it achieves best test accuracy at  $\lambda_3 = 1e - 3$ . We also report the results for SGLD with  $\lambda_3 = 5e - 4$  and  $\lambda_3 = 2e - 3$ .

We report the experimental results in Figure.4. We have the following observations: (1) PL-SGD can achieve higher test accuracy and lower generalization error compared to SGD, which indicates the effectiveness of state-dependent noise. (2) Test result for SGLD can only achieve comparable test accuracy with SGD. Although a larger  $\lambda_3$  leads to lower generalization error compared to SGD, the noise term is too large to converge to low training loss and the test accuracy is worse than SGD for  $\lambda_3 = 1e - 3$  and  $\lambda_3 = 2e - 3$ . So only injecting state-independent Gaussian noise can not improve the test accuracy of SGD with large batch size.

## 6 Conclusion

In this work, we study the dynamics of SGD via investigating state-dependent covariance of the stochastic gradient. We propose power-law dynamic with state-dependent diffusion term to approximate the dynamic of SGD. Based on this characterization, we analyze the escaping efficiency from local minima of power-law dynamic. We prove that power-law dynamic can escape sharp minima exponentially faster than flat minima. We present direct empirical evidence supporting the proposed theoretical results. To the best of our knowledge, this paper is the first to study state-dependent

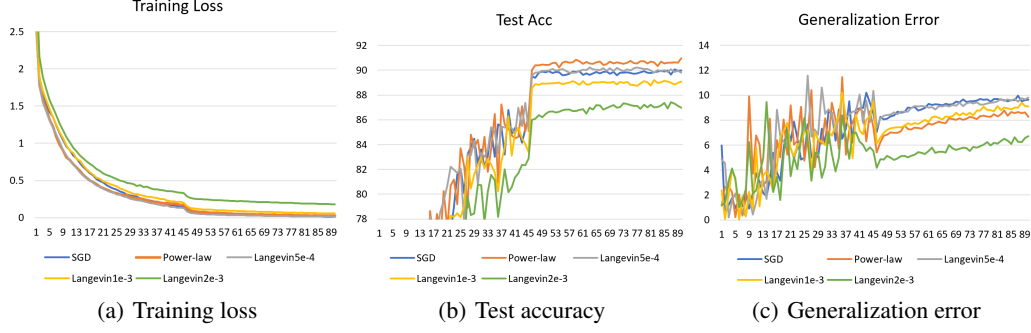


Figure 4: Experimental results on CIFAR-10 with ResNet-18

gradient noise of SGD and we think this work can motivate many interesting research topics on this direction, for example, dynamics of SGD in basin with non-quadratic loss curvatures, non-Gaussian state-dependent noise and new types of state-dependent regularization tricks in deep learning.

## References

- [1] Léon Bottou and Olivier Bousquet. The tradeoffs of large scale learning. In *Advances in neural information processing systems*, pages 161–168, 2008.
- [2] Pratik Chaudhari and Stefano Soatto. Stochastic gradient descent performs variational inference, converges to limit cycles for deep networks. In *2018 Information Theory and Applications Workshop (ITA)*, pages 1–10. IEEE, 2018.
- [3] Anna Choromanska, Mikael Henaff, Michael Mathieu, Gérard Ben Arous, and Yann LeCun. The loss surfaces of multilayer networks. In *Artificial intelligence and statistics*, pages 192–204, 2015.
- [4] Felix Draxler, Kambis Veschgini, Manfred Salmhofer, and Fred Hamprecht. Essentially no barriers in neural network energy landscape. In *International Conference on Machine Learning*, pages 1309–1318, 2018.
- [5] Jiu-Lin Du. Power-law distributions and fluctuation-dissipation relation in the stochastic dynamics of two-variable langevin equations. *Journal of Statistical Mechanics: Theory and Experiment*, 2012(02):P02006, 2012.
- [6] Jeff Z HaoChen, Colin Wei, Jason D Lee, and Tengyu Ma. Shape matters: Understanding the implicit bias of the noise covariance. *arXiv preprint arXiv:2006.08680*, 2020.
- [7] Di He, Yingce Xia, Tao Qin, Liwei Wang, Nenghai Yu, Tie-Yan Liu, and Wei-Ying Ma. Dual learning for machine translation. In *Advances in neural information processing systems*, pages 820–828, 2016.
- [8] Fengxiang He, Tongliang Liu, and Dacheng Tao. Control batch size and learning rate to generalize well: Theoretical and empirical evidence. In *Advances in Neural Information Processing Systems*, pages 1141–1150, 2019.
- [9] Haowei He, Gao Huang, and Yang Yuan. Asymmetric valleys: Beyond sharp and flat local minima. In *Advances in Neural Information Processing Systems*, pages 2549–2560, 2019.
- [10] Kaiming He, Xiangyu Zhang, Shaoqing Ren, and Jian Sun. Delving deep into rectifiers: Surpassing human-level performance on imagenet classification. In *Proceedings of the IEEE international conference on computer vision*, pages 1026–1034, 2015.
- [11] Kaiming He, Xiangyu Zhang, Shaoqing Ren, and Jian Sun. Deep residual learning for image recognition. In *Proceedings of the IEEE conference on computer vision and pattern recognition*, pages 770–778, 2016.

- [12] Wenqing Hu, Chris Junchi Li, Lei Li, and Jian-Guo Liu. On the diffusion approximation of nonconvex stochastic gradient descent. *Annals of Mathematical Sciences and Applications*, 4(1):3–32, 2019.
- [13] Nitish Shirish Keskar, Dheevatsa Mudigere, Jorge Nocedal, Mikhail Smelyanskiy, and Ping Tak Peter Tang. On large-batch training for deep learning: Generalization gap and sharp minima. *arXiv preprint arXiv:1609.04836*, 2016.
- [14] Hao Li, Zheng Xu, Gavin Taylor, Christoph Studer, and Tom Goldstein. Visualizing the loss landscape of neural nets. In *Advances in Neural Information Processing Systems*, pages 6389–6399, 2018.
- [15] Qianxiao Li, Cheng Tai, et al. Stochastic modified equations and adaptive stochastic gradient algorithms. In *Proceedings of the 34th International Conference on Machine Learning-Volume 70*, pages 2101–2110. JMLR. org, 2017.
- [16] Jinlong Liu, Guoqing Jiang, Yunzhi Bai, Ting Chen, and Huayan Wang. Understanding why neural networks generalize well through gsnr of parameters. *arXiv preprint arXiv:2001.07384*, 2020.
- [17] Tianyi Liu, Zhehui Chen, Enlu Zhou, and Tuo Zhao. Toward deeper understanding of nonconvex stochastic optimization with momentum using diffusion approximations. *arXiv preprint arXiv:1802.05155*, 2018.
- [18] Wenlong Mou, Liwei Wang, Xiyu Zhai, and Kai Zheng. Generalization bounds of sgld for non-convex learning: Two theoretical viewpoints. *arXiv preprint arXiv:1707.05947*, 2017.
- [19] Thanh Huy Nguyen, Umut Simsekli, Mert Gurbuzbalaban, and Gaël Richard. First exit time analysis of stochastic gradient descent under heavy-tailed gradient noise. In *Advances in Neural Information Processing Systems*, pages 273–283, 2019.
- [20] Alexander Rakhlin, Ohad Shamir, and Karthik Sridharan. Making gradient descent optimal for strongly convex stochastic optimization. In *Proceedings of the 29th International Conference on Machine Learning*, pages 1571–1578, 2012.
- [21] Akira Satoh. *Introduction to practice of molecular simulation: molecular dynamics, Monte Carlo, Brownian dynamics, Lattice Boltzmann and dissipative particle dynamics*. Elsevier, 2010.
- [22] Tom Schaul, Sixin Zhang, and Yann LeCun. No more pesky learning rates. In *International Conference on Machine Learning*, pages 343–351, 2013.
- [23] Umut Şimşekli, Mert Gürbüzbalaban, Thanh Huy Nguyen, Gaël Richard, and Levent Sagun. On the heavy-tailed theory of stochastic gradient descent for deep neural networks. *arXiv preprint arXiv:1912.00018*, 2019.
- [24] Umut Simsekli, Levent Sagun, and Mert Gurbuzbalaban. A tail-index analysis of stochastic gradient noise in deep neural networks. In *International Conference on Machine Learning*, pages 5827–5837, 2019.
- [25] Constantino Tsallis and Dirk Jan Bukman. Anomalous diffusion in the presence of external forces: exact time-dependent solutions and entropy. *arXiv preprint cond-mat/9511007*, 1995.
- [26] Constantino Tsallis and Dirk Jan Bukman. Anomalous diffusion in the presence of external forces: Exact time-dependent solutions and their thermostistical basis. *Physical Review E*, 54(3):R2197, 1996.
- [27] Nicolaas Godfried Van Kampen. *Stochastic processes in physics and chemistry*, volume 1. Elsevier, 1992.
- [28] Ashish Vaswani, Noam Shazeer, Niki Parmar, Jakob Uszkoreit, Llion Jones, Aidan N Gomez, Łukasz Kaiser, and Illia Polosukhin. Attention is all you need. In *Advances in neural information processing systems*, pages 5998–6008, 2017.

- [29] Jingfeng Wu, Wenqing Hu, Haoyi Xiong, Jun Huan, Vladimir Braverman, and Zhanxing Zhu. On the noisy gradient descent that generalizes as sgd. *arXiv preprint arXiv:1906.07405*, 2019.
- [30] Yuhuai Wu, Mengye Ren, Renjie Liao, and Roger Grosse. Understanding short-horizon bias in stochastic meta-optimization. In *International Conference on Learning Representations*, 2018.
- [31] Han Xiao, Kashif Rasul, and Roland Vollgraf. Fashion-mnist: a novel image dataset for benchmarking machine learning algorithms. *arXiv preprint arXiv:1708.07747*, 2017.
- [32] Zeke Xie, Issei Sato, and Masashi Sugiyama. A diffusion theory for deep learning dynamics: Stochastic gradient descent escapes from sharp minima exponentially fast. *arXiv preprint arXiv:2002.03495*, 2020.
- [33] Guodong Zhang, Lala Li, Zachary Nado, James Martens, Sushant Sachdeva, George Dahl, Chris Shallue, and Roger B Grosse. Which algorithmic choices matter at which batch sizes? insights from a noisy quadratic model. In *Advances in Neural Information Processing Systems*, pages 8194–8205, 2019.
- [34] Mo Zhou, Tianyi Liu, Yan Li, Dachao Lin, Enlu Zhou, and Tuo Zhao. Toward understanding the importance of noise in training neural networks. In *International Conference on Machine Learning*, 2019.
- [35] Yanjun Zhou and Jiulin Du. Kramers escape rate in overdamped systems with the power-law distribution. *Physica A: Statistical Mechanics and its Applications*, 402:299–305, 2014.
- [36] Zhanxing Zhu, Jingfeng Wu, Bing Yu, Lei Wu, and Jinwen Ma. The anisotropic noise in stochastic gradient descent: Its behavior of escaping from sharp minima and regularization effects. In *Proceedings of International Conference on Machine Learning*, pages 7654–7663, 2019.

## 7 Appendix

### 7.1 Proofs for Propositions in Section 3

**Proposition 7** We use  $D(w)$  to denote the covariance matrix of stochastic gradient  $g(w) = g(w^*) + \tilde{H}(w - w^*)$  and  $\tilde{H} = \text{diag}(\tilde{h}_1, \dots, \tilde{h}_d)$  is diagonal. If  $\text{Cov}(\tilde{h}_i, \tilde{h}_j) = 0$  for  $i \neq j$ ,  $\text{Cov}(g_i(w^*), g_j(w^*)) = 0$  for  $i \neq j$  and  $\text{Cov}(g_i(w^*), \tilde{h}_j) = 0, \forall i, j$ , we have  $D(w) = \text{diag}(D_1, \dots, D_d)$  with

$$D_j = \sigma_j + \rho_j(w_j - w_j^*)^2, \quad (15)$$

where  $\sigma_j = \text{Var}(g_j(w^*))$  and  $\rho_j = \text{Var}(\tilde{h}_j)$ .

*Proof:* We use  $D_{ij}$  to denote the element at  $i$ -th row and  $j$ -th column at matrix  $D(w)$ , we have  $D_{ij} = \text{Cov}(g_i(w), g_j(w)) = \text{Cov}(g_i(w^*), g_j(w^*)) + \text{Cov}(\tilde{h}_i, \tilde{h}_j)(w_i - w_i^*)(w_j - w_j^*) + \text{Cov}(g_j(w^*), \tilde{h}_i)(w_i - w_i^*) + \text{Cov}(g_i(w^*), \tilde{h}_j)(w_j - w_j^*)$ . If  $\text{Cov}(\tilde{h}_i, \tilde{h}_j) = 0$  for  $i \neq j$ ,  $\text{Cov}(g_i(w^*), g_j(w^*)) = 0$  for  $i \neq j$  and  $\text{Cov}(g_i(w^*), \tilde{h}_j) = 0, \forall i, j$ , we have  $D_{ij} = 0, i \neq j$ . The  $j$ -th diagonal element is  $D_j = \text{Var}(g_j(w^*)) + \text{Var}(\tilde{h}_j)(w_j - w_j^*)^2$ .  $\square$

**Example:** Consider linear regression with loss function  $L(w) = \frac{1}{2n} \sum_{m=1}^n (x_m w - y_m)^2 = \frac{1}{2n} \|Xw - Y\|_2^2$ . We suppose the output  $y$  is generated as:  $y = w'x + \epsilon$  where  $\epsilon$  is a standard Gaussian random variable, which is independent with the distribution of the input  $x$ . The stochastic gradient at the empirical minimizer  $w^*$  is calculated as  $g(w^*) = \frac{1}{b} \tilde{H}(w^* - w') - \frac{1}{b} \tilde{X}^T \tilde{\epsilon}$ , where  $\frac{1}{b} \tilde{H} = \frac{1}{b} \tilde{X}^T \tilde{X} = \text{diag}(\tilde{h}_1, \dots, \tilde{h}_d)$  and  $\tilde{X}$  is a  $b \times d$  matrix composed by a minibatch of input. We claim that the conditions on  $\text{Cov}(\tilde{h}_i, \tilde{h}_j)$ ,  $\text{Cov}(g_i(w^*), g_j(w^*))$  and  $\text{Cov}(g_i(w^*), \tilde{h}_j)$  in Proposition 7 can be satisfied if  $\text{Cov}(X_i, X_j) = \frac{1}{n} \sum_{m=1}^n x_{m,i} x_{m,j} - (\frac{1}{n} \sum_{m=1}^n x_{m,i})(\frac{1}{n} \sum_{m=1}^n x_{m,j}) = 0, i \neq j$  and the training data is sufficiently large such that  $w^* - w' \approx 0$ .

Suppose that each input follows Gaussian distribution, and  $Cov(X_i, X_j) = 0$  means  $X_i, X_j$  are independent with each other when  $i \neq j$ . Then we have  $Cov(\tilde{h}_i, \tilde{h}_j) = \frac{1}{b} \cdot Cov(X_i^2, X_j^2) = 0$  because the independence of  $X_i, X_j$ .

As for  $Cov(g_i(w^*), g_j(w^*))$ , we have  $Cov(g_i(w^*), g_j(w^*)) = Cov(\tilde{h}_i, \tilde{h}_j)(w_i^* - w_i')(w_j^* - w_j') + Cov(\frac{1}{b}\tilde{X}_j\tilde{\epsilon}, \tilde{h}_i)(w_i^* - w_i') + Cov(\frac{1}{b}\tilde{X}_i\tilde{\epsilon}, \tilde{h}_j)(w_j^* - w_j') + Cov(\frac{1}{b}\tilde{X}_i\tilde{\epsilon}, \frac{1}{b}\tilde{X}_j\tilde{\epsilon})$ . Because the independence of  $X_i$  and  $X_j$ , we have  $Cov(g_i(w^*), g_j(w^*)) = 0$ .

As for  $Cov(g_i(w^*), \tilde{h}_j)$ , we have  $Cov(g_i(w^*), \tilde{h}_j) = Cov(\tilde{h}_i, \tilde{h}_j)(w_i^* - w_i') + Cov(\frac{1}{b}\tilde{X}_j\tilde{\epsilon}, \tilde{h}_j)$ . Because we assume  $w_i^* - w_i'$  approaches zero and  $\epsilon$  is independent with the input, we have  $Cov(g_i(w^*), \tilde{h}_j) \approx 0$ .

Next, we prove Proposition 2, which shows the distribution density of  $w_t$  that satisfied power-law dynamic. The power-law dynamic is defined as

$$dw_t = -H(w_t - w^*)dt + \sqrt{\eta D(w_t)}dB_t, \quad (16)$$

where  $H = diag(h_1, \dots, h_d)$ ,  $D(w) = diag(D_1, \dots, D_d)$  with  $D_j = \sigma_j + \rho_j(w_j - w_j^*)$ .

**Proposition 8** Suppose  $w_t$  satisfies the power-law dynamic in Eq.(16), and the initial point is  $w_0$ . The distribution density of  $w_t$  is  $p(w, t) = \prod_{j=1}^d p(w_j, t)$ , where

$$p(w_j, t) = Z_j(t)^{-1} [1 + \beta_j(t)\kappa_j(w_j - \hat{w}_j(t))^2]^{-\frac{1}{\kappa_j}} \quad (17)$$

with  $\kappa_j = \frac{\eta\rho_j}{h_j}$ ,  $\hat{w}_j(t) = w_j^* + (w_{0,j} - w_j^*)e^{-h_j t}$ ,  $Z_j(t) = [-\frac{1}{K_j}e^{-t/c_j} + \frac{1}{K_j}]^{\frac{1}{2-\kappa_j}}$ ,  $K_j = \frac{h_j}{2\eta\sigma_j\gamma_j}$ ,  $c_j = \frac{1}{h_j(2-\kappa_j)}$ ,  $\beta_j(t) = \gamma_j \left(\frac{1}{Z_j(t)}\right)^2$ ,  $\gamma_j = \frac{(B(\frac{1}{2}, \frac{1}{\kappa_j} - \frac{1}{2}))^2}{\kappa_j}$ .

*Proof:* We use  $\phi_j(w_j) = \frac{\eta D_j(w_j)}{2}$ , the probability density  $p(w, t)$  satisfies the Smoluchowski equation:

$$\frac{\partial p(w, t)}{\partial t} = \sum_{j=1}^d \frac{\partial}{\partial w_j} (h_j(w_j - w_j^*) \cdot p(w, t)) + \sum_{j=1}^d \frac{\partial}{\partial w_j} \left( \phi_j(w_j) \frac{\partial}{\partial w_j} (p(w, t)) \right) \quad (18)$$

$$= \sum_{j=1}^d \frac{\partial}{\partial w_j} (h_j(w_j - w_j^*) \cdot p(w, t)) + \frac{\eta\sigma_j}{2} \sum_{j=1}^d \frac{\partial}{\partial w_j} \left( (1 + \beta_j\kappa_j(w_j - w_j^*)^2) \cdot \frac{\partial}{\partial w_j} (p(w, t)) \right), \quad (19)$$

where  $\kappa_j = \frac{\eta\rho_j}{h_j}$ ,  $\beta_j = \frac{2}{\eta\sigma_j}$ . According to the result for 1-dimensional case in [35], we have  $p(w_j, t) = Z_j(t)^{-1} (1 + \beta_j(t)\kappa_j(w_j - \hat{w}_j(t))^2)^{-\frac{1}{\kappa_j}}$ . For the expression of  $\hat{w}_j(t)$ , it is obtained by solving the ODE  $dw_t = -H(w_t - w^*)dt$ . So we have  $\hat{w}_j(t) = w_j^* + (w_{0,j} - w_j^*)e^{-h_j t}$ . For the expression of  $\beta_j(t)$  and  $Z_j(t)$ , we introduce a result in [25].

If the probability density  $p(w, t)$ ,  $w \in \mathbb{R}$  satisfies  $\frac{\partial}{\partial t} p(w, t) = \frac{\partial}{\partial w} (k_2 x - k_1) p(w, t) + C \frac{\partial^2}{\partial w^2} p(w, t)^\nu$ , its solution will be  $p(w, t) = Z(t)^{-1} (1 - \beta(t)(1 - q)(w - w_M(t))^2)^{\frac{1}{1-q}}$ , where  $q = 2 - \nu$ ,  $Z(t) = Z(0) \left( (1 - \frac{1}{K}) e^{-t/c} + \frac{1}{K} \right)^{\frac{1}{1+\nu}}$  with  $K = \frac{k_2}{2\nu C \gamma (Z(0))^{-\nu-1}}$ ,  $c = \frac{1}{k_2(1+\nu)}$ ,  $\beta(t)Z(t)^2 = \gamma, \forall t$ .

Applying the above result to 1-dimensional case for Eq.(19) (i.e.,  $d=1$ ), we have  $k_1 = hw^*$ ,  $k_2 = h$ ,  $q = \kappa + 1$ ,  $\nu = 1 - \kappa$ .  $Z(t)$  can be rewritten as  $Z(t) = \left( (Z(0))^{1+\nu} - \frac{Z(0)^{1+\nu}}{K} \right) e^{-t/c} + \frac{Z(0)^{1+\nu}}{K} = \left( (Z(0))^{1+\nu} - \frac{2\nu C \gamma}{k_2} \right) e^{-t/c} + \frac{2\nu C \gamma}{k_2}$ . Since  $w_t$  starts at a fixed point, it is a  $\delta$  distribution at  $w_0$ . So  $Z(0) = 0$ . Then  $Z(t)$  has the form  $Z(t) = \left( -\frac{1}{K} e^{-t/c} + \frac{1}{K} \right)$ ,  $K = \frac{k_2}{2\nu C \gamma}$ .

Finally, we calculate what  $C$  and  $\gamma$  are for 1-dimensional case for Eq.(19). Eq.(19) for 1-dimensional case can be rewritten as

$$\frac{\partial p(w, t)}{\partial t} = \frac{\partial}{\partial w} h(w - w^*) \cdot p(w, t) + \frac{\eta\sigma}{(1 - \kappa_j)} \frac{\partial^2}{\partial w^2} p(w, t)^{1-\kappa_j}, \quad (20)$$

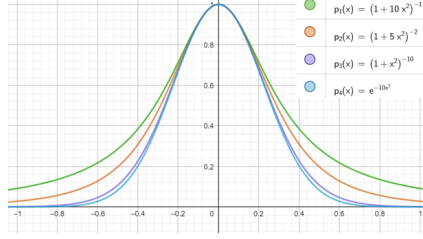


Figure 5: Probability density for power-law dynamic.

because  $(1 + \beta_j \kappa_j (w_j - w_j^*)^2) \propto p(w)^{-\kappa_j}$ . Thus we have  $C = \frac{\eta\sigma}{(1-\kappa_j)}$ .

As for  $\gamma$ , for fixed  $t$ , we have

$$\begin{aligned} 1 &= \int_{-\infty}^{\infty} Z(t)^{-1} (1 + \beta(t) \kappa (w - w_M(t))^2)^{-1/\kappa} dw \\ &= \frac{Z(t)^{-1}}{\sqrt{\beta(t) \kappa}} \int_0^{\infty} y^{-1/2} (1 + y)^{-1/\kappa} dy = \frac{2B(\frac{1}{2}, \frac{1}{\kappa} - \frac{1}{2})}{Z(t) \sqrt{\beta(t) \kappa}}, \end{aligned}$$

where the last equation is established according to Beta distribution. So we have  $\gamma = \frac{B(\frac{1}{2}, \frac{1}{\kappa} - \frac{1}{2})^2}{\kappa}$ .

Because each dimension evolves independently, we have  $p(w, t) = \prod_{j=1}^d p(w_j, t)$ . Combining all the above results together, we can get the result in Proposition.  $\square$

We plot the un-normalized distribution density for 1-dimensional power-law dynamics with different  $\kappa$  in Figure 5. For the four curves, we set  $\beta = 10$ . We set  $\kappa = 1, 0.5, 0.1, 0$  and use green, red, purple and blue line to illustrate their corresponding density function, respectively. When  $\kappa = 0$ , it is Gaussian distribution. From the figure, we can see that the tail for  $\kappa$ -distribution is heavier than Gaussian distribution.

## 7.2 Proofs for Theorems in Section 4

**Theorem 9** Suppose that  $w_t$  follows the power-law dynamic in Eq.(16), we have  $\mathbb{E}[(w_t - w^*)^2] = \mathcal{O}(\sum_{j=1}^d (\eta\sigma_j t)^{\frac{2}{2-\kappa_j}})$ , where  $\kappa_j = \frac{\eta\rho_j}{h_j} < \frac{2}{3}$ . where  $\kappa_j = \frac{\eta\rho_j}{h_j} < \frac{2}{3}$ . The upper bound for  $\epsilon$ -escaping time is  $\mathcal{O}\left(\frac{\epsilon^{2-\min_j \kappa_j}}{\text{Tr}(\Sigma)}\right)$ , where  $\Sigma = \text{diag}(\eta\sigma_1, \dots, \eta\sigma_d)$  and  $\text{Tr}(\cdot)$  denote the trace of the matrix.

*Proof:* According to Proposition 2, the distribution density of  $w_{t,j}$  when it starts at  $w^*$  follows the power-law distribution  $p(w_j, t) = Z_j(t)^{-1} [1 + \beta_j(t) \kappa_j (w_j - w_j^*)^2]^{-\frac{1}{\kappa_j}}$ , where  $\kappa_j, Z_j(t)$  and  $\beta_j(t)$  are defined in Proposition 2. The second-order moment can be calculated as

$$\begin{aligned} \mathbb{E}[(w_{t,j} - w_j^*)^2] &= \int_{-\infty}^{\infty} (w_{t,j} - w_j^*)^2 \cdot Z_j(t)^{-1} [1 + \beta_j(t) \kappa_j (w_{t,j} - w_j^*)^2]^{-\frac{1}{\kappa_j}} dw_{t,j} \\ &\stackrel{v=\beta_j(t)\kappa_j(w_{t,j}-w_j^*)^2}{=} \frac{1}{Z_j(t)(\beta_j(t)\kappa_j)^{\frac{3}{2}}} \int_0^{\infty} v^{\frac{1}{2}} (1+v)^{-\frac{1}{\kappa_j}} dv \\ &\stackrel{v'=\frac{v}{1+v}}{=} \frac{1}{Z_j(t)(\beta_j(t)\kappa_j)^{\frac{3}{2}}} \int_0^1 v'^{\frac{1}{2}} (1-v')^{\frac{1}{\kappa_j}-\frac{5}{2}} dv' \\ &= \frac{B(\frac{3}{2}, \frac{1}{\kappa_j} - \frac{3}{2})}{Z_j(t)(\beta_j(t)\kappa_j)^{\frac{3}{2}}}, \end{aligned}$$

where the last equation is established according to Beta distribution.

According to Proposition 2,  $\kappa_j = \frac{\eta\rho_j}{h_j}$ ,  $Z_j(t) = [-\frac{1}{K_j}e^{-t/c_j} + \frac{1}{K_j}]^{\frac{1}{2-\kappa_j}}$ ,  $K_j = \frac{h_j}{2\eta\sigma_j\gamma_j}$ ,  $c_j = \frac{1}{h_j(2-\kappa_j)}$ ,  $\beta_j(t) = \gamma_j \left(\frac{1}{Z_j(t)}\right)^2$ ,  $\gamma_j = \frac{(B(\frac{1}{2}, \frac{1}{\kappa_j} - \frac{1}{2}))^2}{\kappa_j}$ . Then we have

$$\begin{aligned}\mathbb{E}[(w_{t,j} - w_j^*)^2] &= \frac{B(\frac{3}{2}, \frac{1}{\kappa_j} - \frac{3}{2})}{(B(\frac{1}{2}, \frac{1}{\kappa_j} - \frac{1}{2}))^3} Z_j(t)^2 = \frac{B(\frac{3}{2}, \frac{1}{\kappa_j} - \frac{3}{2})}{(B(\frac{1}{2}, \frac{1}{\kappa_j} - \frac{1}{2}))^3} \left(-\frac{1}{K_j}e^{-t/c_j} + \frac{1}{K_j}\right)^{\frac{2}{2-\kappa_j}} \\ &\stackrel{t \text{ is small}}{\approx} \frac{B(\frac{3}{2}, \frac{1}{\kappa_j} - \frac{3}{2})}{(B(\frac{1}{2}, \frac{1}{\kappa_j} - \frac{1}{2}))^3} \left(\frac{1}{K_j c_j} t\right)^{\frac{2}{2-\kappa_j}} \\ &= \frac{B(\frac{3}{2}, \frac{1}{\kappa_j} - \frac{3}{2})}{(B(\frac{1}{2}, \frac{1}{\kappa_j} - \frac{1}{2}))^3} (2(2-\kappa_j)\eta\sigma_j\gamma_j)^{\frac{2}{2-\kappa_j}} t^{\frac{2}{2-\kappa_j}} \\ &= \mathcal{O}((\eta\sigma_j t)^{\frac{2}{2-\kappa_j}})\end{aligned}$$

Thus we have  $\mathbb{E}[(w_t - w^*)^2] = \mathcal{O}(\sum_{j=1}^d (\eta\sigma_j t)^{\frac{2}{2-\kappa_j}}) \leq \mathcal{O}(Tr(\Sigma)t^{\frac{2}{2-\min_j \kappa_j}})$ . Let  $\mathbb{E}[\|w_t - w^*\|^2] = \epsilon^2$ , we have  $t \leq \mathcal{O}\left(\frac{\epsilon^{2-\min_j \kappa_j}}{Tr(\Sigma)}\right)$ .  $\square$

To prove the next theorem, we reformulate the power-law dynamic as

$$dw_t = -\nabla L(w_t)dt + \sqrt{\eta D(w_t)}dB_t, \quad (21)$$

where  $D(w) = \text{diag}(D_1, \dots, D_d)$  with  $D_j = \sigma_j + \mu_j \ell_j(w_j)$ .

**Theorem 10** (High-dim) *The  $\Omega$ -escaping time of the power-law dynamic in Eq.(21) is as below,*

$$\tau = \frac{2\pi\sqrt{|\det(H_b)|}}{(1 - \frac{\eta\mu_e}{4})\sqrt{\det(H_a)}} \cdot \frac{1}{h_{be}} \prod_{j=1}^d \left(1 + \frac{\mu_j}{\sigma_j} \Delta \ell_j\right)^{\frac{2}{\eta\mu_j} - \frac{1}{2}}, \quad (22)$$

where  $h_{be}$  is the only negative eigenvalue of  $H_b$  and  $\det(\cdot)$  denote the determinant of a matrix.<sup>2</sup>

*Proof:* According to [27],  $\Omega$ -escaping time  $\tau$  is expressed as  $\tau = \frac{P(w \in V_a)}{\int_{\Omega} J d\Omega}$ , where  $V_a$  is the volume of basin  $a$ ,  $J$  is the probability current produced by  $P(w \in V_a)$  and  $\int_{\Omega} J d\Omega$  is the probability flux (surface integrals of probability current). We denote  $\kappa_j = \frac{\eta\mu_j}{2}$ ,  $\phi_j(w_j) = \frac{\eta D_j(w_j)}{2}$ . The probability current along the escaping direction  $e$  satisfies the Smoluchowski equation

$$\begin{aligned}-\nabla J_e(w_e, t) &= \frac{\partial}{\partial w_e} (\nabla \ell_e(w_e) \cdot p(w, t)) + \frac{\partial}{\partial w_e} \left( \phi_e(w_e) \frac{\partial p(w, t)}{\partial w_e} \right) \\ &= \frac{\partial}{\partial w_e} \left( \phi_e(w_e) \cdot \left(1 + \frac{\mu_e}{\sigma_e} \ell_e(w_e)\right)^{-\frac{1}{\kappa_e}} \frac{\partial \left( \left(1 + \frac{\mu_e}{\sigma_e} \ell_e(w_e)\right)^{\frac{1}{\kappa_e}} p(w, t) \right)}{\partial w_e} \right).\end{aligned}$$

So we obtain  $J_e(w_e) = -\phi_e(w_e) \cdot \left(1 + \frac{\mu_e}{\sigma_e} \ell_e(w_e)\right)^{-\frac{1}{\kappa_e}} \frac{\partial \left( \left(1 + \frac{\mu_e}{\sigma_e} \ell_e(w_e)\right)^{\frac{1}{\kappa_e}} p(w, t) \right)}{\partial w_e}$ . Because there is no field source on the escape path,  $J_e(w_e)$  is fixed constant on the escape path. Multiplying  $\phi_e(w_e)^{-1} \cdot \left(1 + \frac{\mu_e}{\sigma_e} \ell_e(w_e)\right)^{\frac{1}{\kappa_e}}$  on both sides, we have

$$J_e \cdot \int_a^c \phi_e(w_e)^{-1} \cdot \left(1 + \frac{\mu_e}{\sigma_e} \ell_e(w_e)\right)^{\frac{1}{\kappa_e}} dw_e = - \int_a^c \frac{\partial \left( \left(1 + \frac{\mu_e}{\sigma_e} \ell_e(w_e)\right)^{\frac{1}{\kappa_e}} p(w, t) \right)}{\partial w_e} dw_e \quad (23)$$

$$= -0 + \left(1 + \frac{\mu_e}{\sigma_e} \ell_e(a_e)\right)^{\frac{1}{\kappa_e}} p(a, t) \quad (24)$$

$$= \frac{1}{Z_e(a)}, \quad (25)$$

<sup>2</sup>Without loss of generality, we assume there's no zero eigenvalue in matrix  $H_a$  and  $H_b$ . The result in Theorem 6 can be extended to general case by following the same technique in the work [32].

As for the term  $\int_a^c \phi_e(w_e)^{-1} \cdot \left(1 + \frac{\mu_e}{\sigma_e} \ell_e(w_e)\right)^{\frac{1}{\kappa_e}} dw_e$ , we have

$$\begin{aligned}
& \int_a^c \phi_e(w_e)^{-1} \cdot \left(1 + \frac{\mu_e}{\sigma_e} \ell_e(w_e)\right)^{\frac{1}{\kappa_e}} dw_e \\
&= \frac{2}{\eta \sigma_e} \int_a^c \left(1 + \frac{\mu_e}{\sigma_e} \ell_e(w_e)\right)^{-1 + \frac{1}{\kappa_e}} dw_e \\
&\approx \frac{2}{\eta \sigma_e} \int_c^{b_e} \left(1 + \frac{\mu_e}{\sigma_e} (\ell_e(b_e) - \frac{1}{2} |h_{be}| (w_e - b_e)^2)\right)^{-1 + \frac{1}{\kappa_e}} dw_e \\
&= \frac{2}{\eta \sigma_e} \int_c^{b_e} \left(1 + \frac{\mu_e}{\sigma_e} (\ell_e(b_e) - \frac{1}{2} |h_{be}| (w_e - b_e)^2)\right)^{-1 + \frac{1}{\kappa_e}} dw_e \\
&= \frac{2}{\eta \sigma_e} \left(1 + \frac{\mu_e}{\sigma_e} \ell_e(b)\right)^{-1 + \frac{1}{\kappa_e}} \int_c^{b_e} \left(1 - \frac{\mu_e}{\sigma_e} \cdot \frac{\frac{1}{2} |h_{be}| (w_e - b_e)^2}{1 + \frac{\mu_e}{\sigma_e} \ell_e(b_e)}\right)^{-1 + \frac{1}{\kappa_e}} dw_e \\
&= \frac{4}{\eta \sigma_e} \left(1 + \frac{\mu_e}{\sigma_e} \ell_e(b)\right)^{-1 + \frac{1}{\kappa_e}} \cdot \left(\frac{\frac{1}{2} \frac{\mu_e}{\sigma_e} |h_{be}|}{1 + \frac{\mu_e}{\sigma_e} \ell_e(b_e)}\right)^{-1/2} \int_0^1 y^{-1/2} (1-y)^{-1 + \frac{1}{\kappa_e}} dy \\
&= \frac{4}{\eta \sigma_e} \left(1 + \frac{\mu_e}{\sigma_e} \ell_e(b)\right)^{-\frac{1}{2} + \frac{1}{\kappa_e}} \sqrt{\frac{2}{\mu_e \sigma_e |h_{be}|}} B\left(\frac{1}{2}, \frac{1}{\kappa_e}\right),
\end{aligned} \tag{26}$$

where the third formula is based on the low temperature assumption. Under the low temperature assumption, we can use the second-order Taylor expansion around the saddle point  $b$ .

Under the low temperature assumption, the probability current concentrates along the direction corresponding the negative eigenvalue of  $h_{be}$ , and the probability flux of other directions can be ignored.

So we have  $\int_{\Omega} J d\Omega = J_e \cdot \int_{\Omega} \prod_{j \neq e} p(w_j) d\Omega = \int J_e dw_e \cdot \int_{\Omega} \prod_{j \neq e} \frac{1}{Z_j} \cdot \left(1 + \frac{\mu_j}{\sigma_j} \ell_j(b_j)\right)^{-\frac{1}{\kappa_j}} \left(1 + \frac{\frac{\mu_j h_{bj}}{2\sigma_j} (b_j - w_j)^2}{1 + \frac{\mu_j}{\sigma_j} \ell_j(b_j)}\right)^{-\frac{1}{\kappa_j}} d\Omega$ . By calculating the integral (which is similar with the calculation of Eq.(26)), we have

$$\begin{aligned}
\int_{\Omega} J d\Omega &= \left( Z_e \cdot \left(1 + \frac{\mu_e}{\sigma_e} \ell_e(b_e)\right)^{-\frac{1}{2} + \frac{1}{\kappa_e}} \sqrt{\frac{32}{\mu_e \sigma_e |h_{be}| \eta^2}} B\left(\frac{1}{2}, \frac{1}{\kappa_e}\right) \right)^{-1} \\
&\quad \prod_{j \neq e} \frac{1}{Z_j} \left(1 + \frac{\mu_j}{\sigma_j} \ell_j(b_j)\right)^{\frac{1}{2} - \frac{1}{\kappa_j}} \sqrt{\frac{2\sigma_j}{\mu_j h_{bj}}} B\left(\frac{1}{2}, \frac{1}{\kappa_j} - \frac{1}{2}\right).
\end{aligned}$$

As for the term  $P(w \in V_a)$ , we have  $P(w \in V_a) = \int_{V_a} p(w) dV = \prod_{j=1}^d \frac{1}{Z_j} \left(1 + \frac{\mu_j}{\sigma_j} \ell_j(a_j)\right)^{\frac{1}{2} - \frac{1}{\kappa_j}} \sqrt{\frac{2\sigma_j}{\mu_j h_{aj}}} B\left(\frac{1}{2}, \frac{1}{\kappa_j} - \frac{1}{2}\right)$ , where we use Taylor expansion of  $L(w)$  near local minimum  $a$ .

Combined the results for  $P(w \in V_a)$  and  $\int_{\Omega} J d\Omega$ , we can get the result.  $\square$

### 7.3 Implementation Details of the Experiments

As for the detailed architecture of our CNN in Section 5.1, both *Conv1* and *Conv2* use  $5 \times 5$  kernels with 10 channels and no padding. Dimensions of full connected layer *fc1* and *fc2* are  $1600 \times 50$  and  $50 \times 10$  respectively. The initialization method is the Kaiming initialization [10] in PyTorch. The learning rate of gradient descent is set to be 0.1. After 3000 iterations, GD converges with almost 100% training accuracy and the training loss being  $1e^{-3}$ .

For the approximation experiments on ResNet18 in Section 5.1, we carry out our experiment on stratified random 1000 data of kaggle's dogs-vs-cats dataset. The initialization method is the Kaiming initialization [10] in PyTorch. The learning rate of gradient descent is set to be 0.001. After 10000 iterations, GD converges with 100% training accuracy and the training loss being  $1e^{-3}$ .

As for the experiments for 2-D model, we also calculate coefficient of the second-order term for the quadratic curve shown in Figure.3(b), and its value is roughly 30, which matches the result in Figure.3(c) in the sense that the result for SGD is similar with the result for power-law dynamic with  $\lambda_1 \approx 32$ .